Received: 13 August 2025 | Revised: 3 October 2025 | Accepted: 3 October 2025

DOI: 10.1002/alz.70915

Alzheimer's & Dementia®
THE JOURNAL OF THE ALZHEIMER'S ASSOCIATION

RESEARCH ARTICLE

Locus coeruleus-entorhinal cortex tract integrity is linked to plasma tau and glial fibrillary acidic protein

Yuliya Patsyuk[1] | **Maxime Van Egroo**[1,2] | **Elise Beckers**[1,3] | **Elouise A. Koops**[2] | **Nicholas J. Ashton**[4,5,6,7] | **Shorena Janelidze**[8] | **Kaj Blennow**[4,9] | **Oskar Hansson**[8] | **Henrik Zetterberg**[4,9,10,11,12,13,14] | **Benedikt A. Poser**[15,16] | **Heidi I. L. Jacobs**[1,2]

[1]Faculty of Health, Medicine and Life Sciences, Mental Health and Neuroscience Research Institute, Alzheimer Centre Limburg, Maastricht University, Maastricht, Netherlands

[2]Athinoula A. Martinos Center for Biomedical Imaging, Department of Radiology, Massachusetts General Hospital and Harvard Medical School, Boston, Massachusetts, USA

[3]GIGA-Cyclotron Research Centre-Human Imaging, University of Liège, Liège, Belgium

[4]Department of Psychiatry and Neurochemistry, Institute of Neuroscience and Physiology, The Sahlgrenska Academy at the University of Gothenburg, Mölndal, Sweden

[5]Centre for Age-Related Medicine, Stavanger University Hospital, Stavanger, Norway

[6]King's College London, Institute of Psychiatry, Psychology and Neuroscience, Maurice Wohl Institute Clinical Neuroscience Institute, London, UK

[7]NIHR Biomedical Research Centre for Mental Health and Biomedical Research Unit for Dementia at South London and Maudsley NHS Foundation, London, UK

[8]Clinical Memory Research Unit, Department of Clinical Sciences Malmö, Lund University, Malmö, Sweden

[9]Clinical Neurochemistry Laboratory, Sahlgrenska University Hospital, Mölndal, Sweden

[10]Department of Neurodegenerative Disease, UCL Institute of Neurology, London, UK

[11]UK Dementia Research Institute at UCL, London, UK

[12]Hong Kong Center for Neurodegenerative Diseases, Clear Water Bay, Hong Kong, China

[13]Department of Pathology and Laboratory Medicine, University of Wisconsin School of Medicine and Public Health, Madison, Wisconsin, USA

[14]Wisconsin Alzheimer's Disease Research Center, University of Wisconsin School of Medicine and Public Health, University of Wisconsin-Madison, Madison, Wisconsin, USA

[15]Department of Cognitive Neuroscience, Faculty of Psychology and Neuroscience, Maastricht University, Maastricht, Netherlands

[16]Maastricht Brain Imaging Centre, Faculty of Psychology and Neuroscience, Maastricht University, Maastricht, Netherlands

Funding information: H2020 FET-Open AROMA, Grant/Award Number: 88587; UK Dementia Research Institute, Grant/Award Number: UKDRI-1003; UCLH Biomedical Research Centre; EU Joint Programme – Neurodegenerative Disease Research, Grant/Award Number: JPND2021-00694; Stiftelsen för Gamla Tjänarinnor; Familjen Erling-Perssons Stiftelse; Olav Thon Stiftelsen; Bluefield Project; Swedish State Support for Clinical Research, Grant/Award Number: ALFGBG-71320; European Union's Horizon Europe research and innovation programme, Grant/Award Number: 101053962; Swedish federal government under the ALF agreement, Grant/Award Numbers: ALFGBG-715986, ALFGBG-965240, 2018-Projekt0279; Regionalt Forskningsstöd, Grant/Award Number: 2020–0314; Skånes universitetssjukhus, Grant/Award Number: 2020-O000028; Konung Gustaf V:s och Drottning Victorias Frimurarestiftelse; Cure Alzheimer's Fund; Parkinson foundation of Sweden, Grant/Award Number: 1280/20; Marianne and Marcus Wallenberg Foundation, Grant/Award Number: 2015.0125; Knut och Alice Wallenbergs Stiftelse, Grant/Award Number: 2017–0383; National Institutes of Health (NIH), Grant/Award Numbers: R01AG062559, R01AG06806, R01AG082006, R21AG074220, 1R01AG068398-01; European Union Joint Program for Neurodegenerative Disorders, Grant/Award Number: JPND2019-466-236; Swedish state under the agreement between the Swedish government and the County Councils, the ALF-agreement, Grant/Award Numbers: ALFGBG-715986, ALFGBG-965240, ALFGBG-71320; Hjärnfonden, Grant/Award Numbers: FO2021–0293, FO2022-0270, FO2017-0243, ALZ2022-0006; Swedish Alzheimer Foundation, Grant/Award Numbers: AF-939932, AF-930351, AF-939721, AF-968270; Alzheimer's Drug Discovery Foundation, Grant/Award Numbers: 201809–2016862, 201809-2016615; Vetenskapsrådet, Grant/Award Numbers: 2016–00906, 2017–00915, 2019–02397, 2022–01018, 2023–00356; HORIZON EUROPE Marie Sklodowska-Curie Actions, Grant/Award Numbers: 860197, 101109451-ADEEPSLEEP; BrightFocus Foundation, Grant/Award Number: A20211016F; Alzheimer's Association, Grant/Award Numbers: 23AARF-1026796, AARG-22-920434, ZEN-21-848495; Alzheimer Nederland, Grant/Award Number: WE.03-2019-02; AD Strategic Fund and the Alzheimer's Association, Grant/Award Numbers: ADSF-21-831376-C, ADSF-21-831381-C, ADSF-21-831377-C, ADSF-24-1284328-C

Correspondence
Heidi Jacobs, Athinoula A. Martinos Center for Biomedical Imaging, Department of Radiology, Massachusetts General Hospital/Harvard Medical School, Boston, MA 02114, USA.
Email: hjacobs@mgh.harvard.edu

Abstract

INTRODUCTION: Pretangle tau inclusions from the locus coeruleus (LC) are hypothesized to propagate to the entorhinal cortex (EC) via neuron-to-neuron transmission along its projections. The lower integrity of the LC-EC pathway accompanying Alzheimer's disease (AD) pathology is supported by *post mortem* studies, but in vivo evidence remains limited.

METHODS: We associated diffusion-weighted 7T magnetic resonance imaging (MRI) metrics of microstructural integrity within the LC-EC tract to plasma AD-related biomarkers in a cohort of 47 cognitively unimpaired adults.

RESULTS: Worse overall and local LC-EC integrity, indicated by lower fractional anisotropy (FA) and higher mean diffusivity (MD), was related to elevated concentrations of plasma phosphorylated tau 181 (p-tau181), p-tau217, and glial fibrillary acidic protein (GFAP). A higher orientation dispersion index (ODI) within the LC-EC tract was linked to elevated plasma p-tau181 and p-tau231 levels.

DISCUSSION: The lower integrity of the LC-EC pathway may serve as a key indicator of the earliest AD-related pathophysiological processes to improve detection of at-risk individuals.

KEYWORDS
Alzheimer's disease, biomarkers, diffusion tensor imaging, entorhinal cortex, locus coeruleus, microstructural integrity, magnetic resonance imaging, neurite orientation dispersion and density imaging, preclinical, tau, white matter

Highlights

- Standard DTI model metrics in the LC- EC tract are linked to elevated plasma p-tau and GFAP.
- A higher ODI in the voxels containing the LC-EC tract is related to elevated plasma p-tau.
- LC-EC integrity links to AD-related biomarkers show topographic specificity.
- Lower LC-EC integrity may be a key indicator of the earliest AD-related pathology.

1 | INTRODUCTION

The locus coeruleus (LC) is a small nucleus located bilaterally in the dorsal area of the pons and constitutes the primary source of norepinephrine (NE) for the central nervous system. Through its extensive projections to the whole brain, the LC modulates a series of physiological and cognitive functions, including arousal, attention, emotional regulation, or learning and memory.[1] Importantly, autopsy studies reported that the LC is among the first regions to accumulate phosphorylated tau in Alzheimer's disease (AD), prior to any detectable neocortical involvement and as early as in the first few decades of life.[2–4] It has been proposed that pretangle tau inclusions from the LC propagate to the first cortical site of neuropathological accumulation – the entorhinal cortex (EC) – via neuron-to-neuron transmission along its projections.[5] In addition, *post mortem* studies reported morphological changes in LC neurons such as reduction in fiber density and dendritic arborization in the initial stages of AD,[6] but such evidence in vivo remains limited. Crucially, while a few studies examined the integrity of the LC-EC tract across clinical AD groups,[7–10] the interplay between early AD-related pathophysiological processes and the structural alteration of this key tract remains poorly understood. Investigating the structural integrity of the LC-EC pathway in cognitively unimpaired individuals may therefore shed light on the earliest pathological changes underlying disease progression.

Recent developments in high-resolution magnetic resonance imaging (MRI) now allow for a precise identification of the LC at the individual level.[11,12] In turn, this can be leveraged to improve the estimation of LC efferent projections and identify white matter (WM) fiber bundles forming the LC-EC pathway. This approach can be further refined when combined with multishell, high-angular-resolution

diffusion MRI (dMRI) acquisition, which mitigates crossing fiber limitations inherent in the more traditional diffusion tensor imaging (DTI) model and enables the use of biophysical diffusion models, such as the neurite orientation dispersion and density imaging (NODDI) model, to assess more specific tissue microstructural properties.[13] Given the evidence suggesting that the LC-EC tract is an early predilection pathway contributing to potential proteinopathic transmission processes during the earliest stages of AD, examining LC-EC microstructural integrity in the context of early AD pathology could provide further insights into in vivo detectable pathological events preceding preclinical AD.

Guided by the hypothesis that elevated levels of AD pathology may be associated with fine-grained microstructural changes in the LC-EC, we sought to investigate the microstructural integrity of the pathway using 7T multishell dMRI data and assessed its relation to several plasma AD-related biomarkers in cognitively unimpaired individuals across the adult lifespan.

RESEARCH IN CONTEXT

1. **Systematic review**: A literature review using traditional sources (e.g., PubMed) indicated that integrity of the LC-EC tract is altered in the context of AD-related pathophysiological processes. in vivo neuroimaging evidence relating LC-EC integrity to AD pathologic processes in preclinical stages of the disease remains limited. Investigating the associations between fine-grained changes in the LC-EC pathway, and early AD pathology may facilitate the identification of individuals at greater risk for AD.
2. **Interpretation**: Worse 7T MRI-derived LC-EC tract microstructural integrity metrics are associated with elevated levels of plasma phosphorylated tau and GFAP in cognitively unimpaired adults. These associations show topographical specificity, particularly around bending regions of the tract.
3. **Future directions**: Longitudinal studies using repeated assessment of LC-EC pathway integrity and AD biomarkers will be critical to better understand the pathological mechanisms underlying the observed relationships and to elucidate the temporal ordering of the events at play in asymptomatic individuals.

2 | MATERIALS AND METHODS

2.1 | Participants

A subgroup of cognitively unimpaired individuals across the adult lifespan (n = 47; mean age = 60.4 ± 15.1 years; age range = 30 to 85; 23 females [48.94%]) from the 7T Adult Lifespan Cohort[14–16] was included in the present study based on the availability of diffusion-weighted imaging data. Participants were recruited for the original study from the general population in the southernmost region of the Netherlands. Exclusion criteria included ultra-high-field imaging contraindications, a history of major psychiatric or neurological disorders, history of brain injury or brain surgery, history of major vascular disorders, use of drugs or psychoactive medication, or excessive alcohol consumption (>15 units/week).

2.2 | 7T MRI data acquisition

All participants underwent an imaging protocol on a 7T MAGNETOM Siemens scanner (Siemens Healthineers, Erlangen, Germany) with a 32-channel (1TX/32RX) head coil (Nova Medical, Wilmington, MA, USA). First, a whole-brain magnetization-prepared 2 rapid acquisition gradient-echo (MP2RAGE) sequence[17] (TR = 5000 ms, TE = 2.47 ms, flip angle = 5°/3°, voxel size = 0.7 mm isotropic, number of slices = 240) was acquired. The LC was imaged using an in-house developed magnetization transfer-weighted turbo flash (MT-TFL) sequence[12] multishot 3D readout, repetition time (TR) = 538 ms, echo time (TE) = 4.08, flip angle = 8°, voxel size = 0.4 × 0.4 × 0.5 mm, number of slices = 60, with center-out k-space sampling and preceded by 20 long off-resonant Gaussian sinc pulses (pulse length = 5.12 ms, bandwidth = 250 Hz, B_1 = 0.25 μT). The field of view of the MT-TFL sequence was placed perpendicular to the dorsal surface of the pons and encompassed the area between the inferior colliculi and the caudal border of the pons. A multishell high-angular-resolution DWI sequence (66 directions, b = 2000 s/mm^2; 35 directions, b = 700 s/mm^2; six directions, b = 20 s/mm^2; b = 0 in opposite phase-encoding direction; TR = 5000 ms, TE = 60.8 ms, voxel size = 1.25 mm isotropic, number of slices = 72) was used to acquire diffusion data. Given our focus on the brainstem, the field of view of the DWI acquisitions omitted the dorsal-most part of the frontal/parietal lobes.

2.3 | Structural MRI data preprocessing

Whole-brain MP2RAGE images were processed using FreeSurfer[18] (version 6.0.0; https://surfer.nmr.mgh.harvard.edu) with the software's default protocol for cortical and subcortical reconstruction, as described in Dale et al.,[19] including the expert options for 7T data. Shortly, each T1-weighted image underwent an automated segmentation process including intensity normalization, skull stripping, segregation of the left and right hemispheres, removal of the brainstem and cerebellar areas, correction of topology defects, definition of the borders between gray matter (GM) and WM and between GM and cerebrospinal fluid (CSF), and parcellation of cortical and subcortical areas. Subsequently, all images underwent visual inspection and, if necessary, manual editing. Finally, the parcellated areas were registered to the MP2RAGE space using the function Estimate and Reslice with the nearest neighbor interpolation option in SPM12 software (https://www.fil.ion.ucl.ac.uk/spm/software/spm12/).

A detailed description of our 7T LC preprocessing pipeline can be found in Van Egroo et al. [15,16] In summary, individual MT-TFL scans were intensity-normalized based on a subject-specific mean intensity of a 10 × 10-voxel region of interest (ROI) located in the pontine tegmentum (PT). Next, a study-specific MT-TFL template was created using an iterative diffeomorphic warp estimate in the Advanced Normalization Tools (ANTs) software. The LC mask was then manually delineated on the resulting template by an expert (MVE), based on voxel intensities and prior knowledge of the anatomical properties of the LC.

2.4 | Diffusion MRI data preprocessing

Diffusion-weighted scans were corrected for B_0 susceptibility-induced and eddy current-induced distortions and motion artifacts employing topup and eddy tools of the FSL software[20] (version 5.0.9). Whole-brain maps of DTI-based markers of tissue microstructure such as fractional anisotropy (FA) and mean diffusivity (MD) were computed using FSL's *dtifit* (version 6.0.7.6) on the preprocessed DWI data. NODDI-derived parameter maps of the neurite density index (NDI) and orientation dispersion index (ODI) were obtained using the Microstructure Diffusion Toolbox (version 1.2.6, https://github.com/robbert-harms/MDT). By adopting a tissue model capable of distinguishing three types of microstructural environment, namely, the intracellular, the extracellular, and the free water compartment, the NODDI model allows for a more specific characterization of subvoxel tissue features compared to DTI-based metrices.[13] In particular, NDI values range from 0 to 1, with lower values indicating lower neurite density (i.e., predominantly extracellular diffusion) and higher values indicating high neurite density (i.e., predominantly intracellular diffusion). ODI values range from 0 to 1, with lower values reflecting lower neurite arborization/angular variation (i.e., parallel neurites) and higher values reflecting higher neurite arborization/angular variation (i.e., highly dispersed neurites). Moreover, NODDI can better distinguish different neurobiological processes that may confound DTI metrics at a voxel level: for instance, a reduction in FA may be caused by an underlying reduction in NDI, an increased ODI, or other microstructural changes in the tissue.[21] By leveraging our high-angular, multishell diffusion imaging protocol, the NODDI model allows for the disentanglement and separate analysis of these two key factors contributing to FA.

2.5 | ROI definition and tractography

The LC mask was first brought back from the study-specific MT-TFL template space to the individual structural space using the inverse of the transformations previously calculated by ANTs. The EC ROI was extracted from the FreeSurfer parcellation as per the Desikan–Killiany atlas,[22] while the more fine-grained parcellation provided by the Destrieux atlas was used for the creation of the composite (pre-)frontal areas to be used in the control analysis (Supplementary Methods). Then, individual MP2RAGE images were coregistered to the individual mean diffusion-weighted b0 volume using the SPM12 Estimate and Reslice function with the nearest neighbor interpolation method, and the resulting transformation matrices were applied to the individual LC masks, EC, and (pre-)frontal parcellations to obtain the LC, EC, and (pre-)frontal ROIs into the individual DWI space for subsequent tractography.

The LC-EC tract of interest was obtained, for each subject, by means of unguided probabilistic tractography using FSL's *bedpostx* (a Bayesian estimation of diffusion parameters allowing for crossing-fiber modeling) and *probtrackx* (Figure 1). For *bedpostx*, the number of fiber populations modeled per voxel was increased to 3 from the default value of 2 to better capture the anatomical complexity of the surveyed region, while other options were left at their default values. In *probtrackx*, the LC was set as a seed ROI, while the EC was set as both waypoint and terminative ROI. To obtain the control tract, the (pre-)frontal composite was used as both waypoint and terminative ROI. Additional computing options were left at their default values, except for the curvature threshold, which was decreased from 0.2 (corresponding to a minimum angle of approximately ±80°) to 0.0 to allow for the detection of especially sharp bending points, which characterize the LC-EC tract. The tractography was run separately for each hemisphere. The resulting tracts were binarized and visually inspected to ensure that the tractography outcome was not excessively sparse, uneven, or fragmented. For each subject, the LC-EC tract was further pruned by multiplying a binarized (threshold = 0.05) and dilated (kernel operated by a factor of 3) version of the probabilistic atlas computed by Sun et al.,[9] coregistered to the individual diffusion space. Finally, to avoid redundancies and only examine the WM bundles, we subtracted the LC and EC ROIs from the LC-EC tract and the LC and (pre-)frontal composite ROIs from the control tract.

2.6 | DTI-based and NODDI parameter extraction

FA and MD values computed in *dtifit* and NODDI-derived NDI and ODI metrics were extracted by taking the mean of values across the LC-EC tract. Mean diffusion metrics were averaged across left and right hemispheres, and further statistical analyses were conducted on bilaterally sourced values, as we were not operating under any a priori hypothesis on hemispheric lateralization. The same approach was used to extract DTI and NODDI values in the (pre-)frontal control tract.

2.7 | Slice extraction

To further evaluate any topographical pattern along the LC-EC pathway, we proceeded to extract two-dimensional slices from the individual tracts. Given the shape of the pathway containing points of sharp curvature, we split it into three sections: the caudal-most part, connecting the LC to the thalamic region, was sliced along the *y*-dimension (left hemisphere: $y = -44$ to -14, right hemisphere: $y = -44$ to -13);

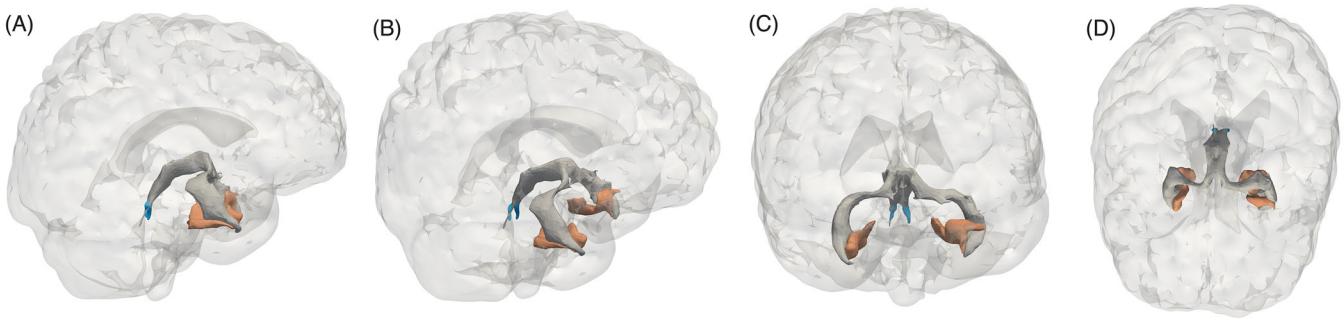

FIGURE 1 LC-EC tract in one representative participant in subject-specific anatomical space. The tract is shown alongside the LC (in blue) and the EC (in orange) in sagittal (A), sagitto-coronal (B), coronal (C), and axial (D) views. EC, entorhinal cortex; LC, locus coeruleus.

the intermediate portion, proceeding laterally toward the temporal lobes, was sliced along the *x*-dimension (left hemisphere: $x = 2$ to -41, right hemisphere: $x = -4$ to 40); the inferior portion, terminating in the EC, was sliced along the *z*-dimension (left hemisphere: $z = -20$ to -48, right hemisphere: $z = -19$ to -47). To ensure consistency in these nodes across participants, we used the binarized version of the Sun atlas of the LC-EC tract[9] by extracting, in the individual space, the overlap between the three sections obtained from the atlas and our individual tracts. To accommodate for anatomical variability across individual tracts in native space and the atlas, we used the dilated version (kernel operated by a factor of 3) of the atlas: this procedure explains the slight discrepancy in LC-EC section coordinates between our work and similar efforts.[7]

2.8 | Plasma AD-related assessments

Fasted EDTA plasma samples were collected through venipuncture in the morning and handled according to the standard operating procedure stipulated by the central biobank of Maastricht University Medical Center. Samples were centrifuged at 2000 × g, aliquoted in polypropylene tubes, and stored at −80°C in the biobank within 60 min of collection. Plasma biomarkers were analyzed in randomized order using ultra-sensitive Single molecule array (Simoa) assays (Quanterix, Inc.) for amyloid beta (Aβ) 42 and Aβ40 (to create Aβ42/40 ratio), phosphorylated tau (p-tau) 181 (p-tau181 V2 Advantage Kit), p-tau231 (University Gothenburg),[23] GFAP (Discovery kits for HD-X), and neurofilament light (NfL) (NF-light Advantage Kit) at the University of Gothenburg (Sweden). Analyses were performed in duplicates using a 1:4 automated dilution protocol for all markers, except for 1:2 dilution protocol for p-tau231. Analysis of plasma p-tau217 was performed at Lund University (Sweden) using the Meso Scale Discovery (MSD) platform as previously described.[24] Apolipoprotein E (*APOE*) genotyping was performed using polymerase chain reaction on deoxyribonucleic acid extracted from blood samples, and a participant's *APOE* status was defined as "ε4 carrier" if they carried at least one ε4 allele. Technicians handling the blood samples were blinded to participant imaging data, and staff collecting imaging data were blinded to blood assessment results.

2.9 | Statistical analyses

All analyses were performed using R statistical software (version 4.4.1, https://www.r-project.org/). As an initial data check, we performed zero-order correlations across all relevant variables with Pearsons correlations and then used robust multiple linear regression models (using the rlm function in the MASS package [version 7.3-61], fitted using iterated reweighted least squares implementing a Huber M-estimator; the corresponding *p* values were extracted using the "f.robftest" function in the sfsmisc package [version 1.1-19]) to account for potential outliers in biomarkers. Following our main hypothesis, we examined the relationship between DTI-derived (namely, FA and MD) or NODDI-derived (namely, NDI and ODI) metrics in the LC-EC tract and plasma AD-related biomarkers (NfL, GFAP, Aβ42/40 ratio, p-tau181, p-tau217, and p-tau231). All models were corrected for age, sex, and tract volume and adjusted for multiple comparisons. Sensitivity analyses were conducted by repeating the models in a subsample of older (≥50 years) individuals ($N = 35$) and by adding *APOE* status as a covariate. To determine the specificity of our results, we examined similar associations on the control tract in the entire sample. In a second step, we performed slice-wise associations to explore the topographic distribution. The slices were pooled per three consecutive slices, resulting in 32 bilateral bins, and the associations described were evaluated within each bin.

3 | RESULTS

3.1 | Participant characteristics

Demographic characteristics of the study sample are reported in Table 1. The mean age of the participants was 60 years (range, 30 to 85 years), 23 were females (49%) and 11 (23%) were carriers of at least one *APOE* ε4 allele.

TABLE 1 Summary statistics for demographic characteristics, diffusion metrics and plasma biomarker levels in the study sample.

	N = 47
Demographic characteristics	
Age, years	60.43 ± 15.11 (30 to 85)
Sex, no. (%)	
Female	23 (48.94)
Male	24 (51.06)
APOE ε4 carrier, no. (%)	11 (23.40)
Volume LC-EC bilateral (mm^3)	4490.46 ± 1775.49 (1364.52 to 10,552.68)
Volume control tract bilateral (mm^3)	65,753.31 ± 17393.89 (31,364.53–105,552.07)
Diffusion metrics	
LC-EC tract (bilateral)	
FA	0.38 ± 0.02 (0.34 to 0.44)
MD (10^3)	0.64 ± 0.026 (0.59 to 0.71)
NDI	0.59 ± 0.04 (0.49 to 0.67)
ODI	0.23 ± 0.02 (0.18 to 0.27)
Control tract (bilateral)	
FA	0.45 ± 0.02 (0.38 to 0.51)
MD (10^3)	0.58 ± 0.03 (0.53 to 0.67)
NDI	0.65 ± 0.05 (0.51 to 0.72)
ODI	0.22 ± 0.02 (0.15 to 0.25)
Plasma biomarkers	
GFAP (pg/mL)	153 ± 63.8 (53.8 to 389)
NfL (pg/mL)	18.1 ± 7.68 (6.56 to 43.4)
Aβ42/40 ratio	0.09 ± 0.01 (0.05 to 0.12)
p-tau181 (pg/mL)	1.68 ± 0.86 (0.86 to 6.44)
p-tau217 (pg/mL)	0.27 ± 0.13 (0.11 to 0.81)
p-tau231 (pg/mL)	8.34 ± 3.87 (3.29 to 25.8)

Note: Summary statistics for demographic characteristics, diffusion metrics, and plasma biomarker levels in the study sample. Values are presented as mean ± SD (range) for continuous variables and percentages for dichotomous variables.

Abbreviations: Aβ, amyloid beta; *APOE* ε4, apolipoprotein ε4; EC, entorhinal cortex; FA, fractional anisotropy; GFAP, glial fibrillary acidic protein; LC, locus coeruleus; MD, mean diffusivity (10^3); NDI, neurite density index; NfL, neurofilament light polypeptide; ODI, orientation dispersion index.

3.2 | Correlations of demographics with plasma AD-related biomarkers and LC-EC tract diffusion metrics

Older individuals exhibited lower Aβ42/40 ($t = -3.54$, $p < 0.001$) and higher GFAP ($t = 4.92$, $p < 0.001$), NfL ($t = 7.07$, $p < 0.001$), and p-tau181 ($t = 2.36$, $p = 0.02$) levels (Table S1). Females displayed higher MD ($t = -2.68$, $p = 0.01$) within the LC-EC tract. Older age was associated with lower ODI ($t = -2.91$, $p = 0.006$) in the LC-EC tract. Age and sex differences remained significant when further controlling for *APOE* ε4 status

3.3 | Whole-tract relationships between LC-EC tract diffusion metrics and plasma AD-related biomarkers

Lower FA in the LC-EC pathway was associated with higher levels of GFAP ($t = -2.24$, $p = 0.03$, false discovery rate (FDR)-adjusted p value [p_{FDR}] = 0.06) and p-tau217 ($t = -2.07$, $p = 0.04$, $p_{FDR} = 0.09$). Conversely, MD was positively associated with GFAP ($t = 3.81$, $p < 0.001$, $p_{FDR} = 0.002$), p-tau181 ($t = 2.40$, $p = 0.02$, $p_{FDR} = 0.08$), and p-tau217 ($t = 2.21$, $p = 0.03$, $p_{FDR} = 0.09$). Higher ODI in the LC-EC tract was related to elevated p-tau181 ($t = 2.09$, $p = 0.04$, $p_{FDR} = 0.08$) and p-tau231 ($t = 2.49$, $p = 0.02$, $p_{FDR} = 0.07$) (Figure 2, Table 2). No significant relationships were found with NfL values, Aβ42/40 ratio, or NDI values in the LC-EC tract. To examine the specificity of these findings to the LC-EC tract, all analyses were repeated in the control tract, where we observed that a lower Aβ42/40 ratio was associated with lower FA ($t = 3.32$, $p = 0.003$, $p_{FDR} = 0.06$), lower NDI ($t = 2.19$, $p = 0.04$, $p_{FDR} = 0.05$), and higher MD ($t = -3.20$, $p = 0.003$, $p_{FDR} = 0.006$) values, but we detected no significant associations with the other plasma markers (Figure S1; Table S2).

3.4 | Slice-wise relationships between LC-EC tract diffusion metrics and plasma AD-related biomarkers

Taking a more granular approach by using a slice-wise approach along the LC-EC pathway, we observed that the associations involving GFAP, p-tau217, and p-tau231 were driven by the portion of the tract immediately following the medial bend (Figure 3, first vertical dotted line), right after exiting the thalamic area and proceeding towards the temporal lobes, the region around the curvature point leading the pathway to its inferior portion (Figure 3, second vertical dotted line) and the final part of the tract, terminating in the EC. MD associations were mostly observed in the final portion of the tract, close to the EC, whereas the associations involving FA and ODI were more pronounced in the starting region of the tract, from the LC toward the thalamic region.

4 | DISCUSSION

The LC is one of the earliest sites of accumulation of tau pathology, and has been proposed to play a crucial role in the propagation of tau to the first affected cortical site – the EC – via neuron-to-neuron transmission.[25,26] This seeding process is thought to emerge decades before the onset of AD clinical symptoms.[2] While supported by *post mortem*[6,27] and animal[28,29] studies, in vivo evidence in humans remains limited due to the complexities in accurately identifying the LC and its sharp-bending WM bundle to the EC. Here, by combining recent advances in plasma AD-related biomarkers with dedicated LC

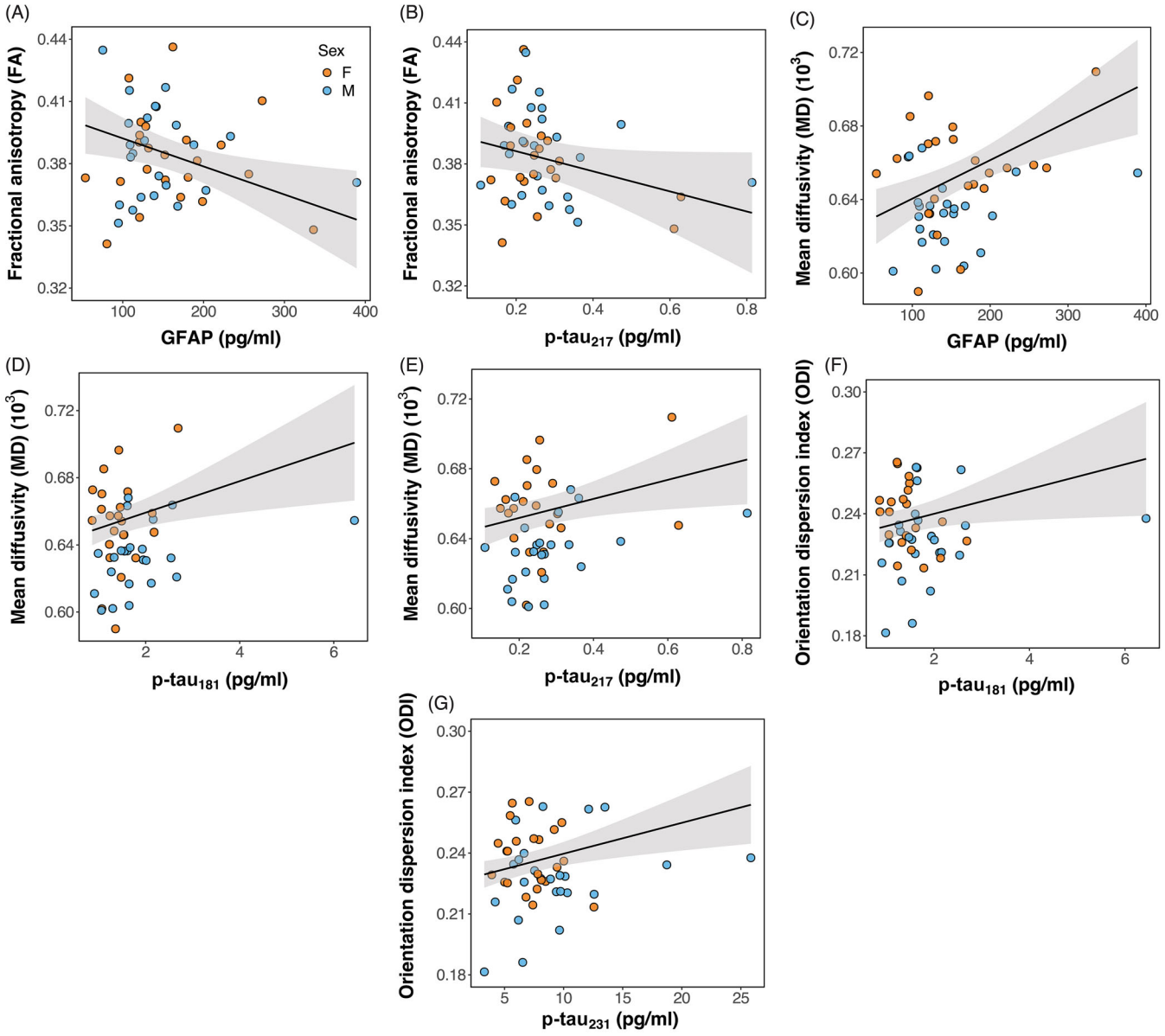

FIGURE 2 Associations between plasma Alzheimer's disease (AD)-related biomarkers ($N = 47$) and LC-EC tract integrity metrics of FA (A, B), MD (C-E) and ODI (F, G). Females are indicated in orange, males in blue. Shaded areas surrounding the regression lines represent the 95% confidence interval of the regression fit. See Table 2 for all the regression coefficients. EC, entorhinal cortex; FA, fractional anisotropy; GFAP, glial fibrillary acidic protein; LC, locus coeruleus; MD, mean diffusivity; ODI, orientation dispersion index.

imaging as well as conventional (DTI) and advanced (NODDI) diffusion models at ultra-high field in vivo, we showed that lower LC-EC tract microstructural integrity was associated with hyperphosphorylated tau burden and astrogliosis in cognitively unimpaired individuals. These results emphasize the potential of microstructural changes within the LC-EC tract as a critical indicator of the earliest AD-related pathophysiological events.

First, we observed that worse LC-EC tract integrity, indicated by lower FA and higher MD values, was related to elevated concentrations of plasma p-tau181 and p-tau217. Similarly, higher ODI within the LC-EC tract was associated with elevated plasma p-tau181 and p-tau231 levels. While p-tau181 is well established for the detection of existing AD pathology,[30,31] p-tau217 has shown promise as a sensitive marker for earlier detection of AD,[32] potentially offering increased accuracy in detecting AD pathology and higher predictive value for predicting disease trajectory.[33,34] On the other hand, the p-tau231 epitope reflects a very early detectable process preceding preclinical AD, signaling tau features that precede the formation of neurofibrillary tangles.[35] Furthermore, recent work demonstrated the ability of p-tau231 to distinguish positron emission tomography (PET)-derived Braak stage 0 from Braak stages I and II, whereas p-tau181 fails to do so.[23] Our findings, obtained in a cognitively unimpaired cohort, expand on prior reports of lower WM integrity within the LC-EC tract correlating with more advanced clinical AD stages using other diffusion-based

TABLE 2 Associations between LC-EC diffusion metrics and plasma AD-related biomarkers.

	FA																	
	GFAP			NfL			Aβ42/40			p-tau181			p-tau$_{217}$			p-tau231		
	t	*p*	p_{FDR}	*t*	*p*	p_{FDR}	*t*	*p*	p_{FDR}	*t*	*p*	p_{FDR}	*t*	*p*	p_{FDR}	*t*	*p*	p_{FDR}
Biomarker	−2.24	**0.03**	0.06	−0.44	0.66	0.89	1.37	0.18	0.36	−1.43	0.16	0.21	−2.07	**0.04**	0.09	−0.76	0.45	0.60
Age	2.04	0.05		0.94	0.35		0.17	0.167		1.34	0.19		1.38	0.18		1.07	0.30	
Male sex	−0.66	0.51		0.14	0.89		0.77	0.767		0.50	0.62		0.19	0.85		0.35	0.73	
Tract volume	−2.46	**0.03**		−1.79	0.08		0.23	0.226		−1.78	0.08		−1.81	0.08		−1.75	0.09	
	MD																	
	GFAP			NfL			Aβ42/40			p-tau181			p-tau217			p-tau231		
	t	*p*	p_{FDR}	*t*	*p*	p_{FDR}	*t*	*p*	p_{FDR}	*t*	*p*	p_{FDR}	*t*	*p*	p_{FDR}	*t*	*p*	p_{FDR}
Biomarker	3.81	**<0.001**	**0.002**	1.67	0.10	0.39	−1.51	0.13	0.36	2.40	**0.02**	0.08	2.21	**0.03**	0.09	0.79	0.43	0.60
Age	−3.67	**0.00**		−2.32	**0.03**		−2.11	**0.04**		−1.82	0.07		−1.83	0.07		−1.67	0.10	
Male sex	−2.32	**0.03**		−3.05	**0.00**		−3.49	**0.001**		−3.67	**0.00**		−3.34	**0.002**		−3.13	**0.003**	
Tract volume	2.94	**0.01**		1.90	0.06		1.86	0.07		2.61	**0.01**		2.26	**0.03**		2.06	**0.05**	
	NDI																	
	GFAP			NfL			Aβ42/40			p-tau181			p-tau217			p-tau231		
	t	*p*	p_{FDR}	*t*	*p*	p_{FDR}	*t*	*p*	p_{FDR}	*t*	*p*	p_{FDR}	*t*	*p*	p_{FDR}	*t*	*p*	p_{FDR}
Biomarker	−1.07	0.28	0.28	−0.04	0.97	0.97	0.97	0.33	0.42	−0.07	0.95	0.95	−0.44	0.66	0.66	0.43	0.66	0.66
Age	−0.24	0.81		−0.78	0.44		−0.54	0.59		−1.50	0.15		−1.06	0.30		−1.27	0.21	
Male sex	−0.28	0.78		−0.05	0.96		0.09	0.93		−0.18	0.86		−0.01	0.99		−0.16	0.87	
Tract volume	−0.90	0.37		−0.84	0.40		−0.62	0.53		−1.08	0.28		−0.83	0.41		−0.90	0.37	
	ODI																	
	GFAP			NfL			Aβ42/40			p-tau181			p-tau217			p-tau231		
	t	*p*	p_{FDR}	*t*	*p*	p_{FDR}	*t*	*p*	p_{FDR}	*t*	*p*	p_{FDR}	*t*	*p*	p_{FDR}	*t*	*p*	p_{FDR}
Biomarker	−1.18	0.27	0.28	0.43	0.67	0.89	−0.80	0.42	0.42	2.09	**0.04**	0.08	1.08	0.28	0.38	2.49	**0.02**	0.07
Age	−1.61	0.12		−2.26	**0.03**		−2.91	**0.01**		−4.25	**<0.001**		−3.14	**0.003**		−4.06	**<0.001**	
Male sex	−1.54	0.13		−1.06	0.29		−1.16	0.25		−1.93	0.06		−1.12	0.27		−1.99	0.06	
Tract volume	0.80	0.41		0.56	0.58		0.45	0.65		0.53	0.60		0.58	0.56		0.58	0.56	

Note: Associations between LC-EC diffusion metrics and plasma AD biomarkers.

Abbreviations: Aβ, amyloid-beta; EC, entorhinal cortex; FA, fractional anisotropy; GFAP, glial fibrillary acidic protein; LC, coeruleus; MD, mean diffusivity; NDI, neurite density index; NfL, neurofilament light polypeptide; ODI, orientation dispersion index.

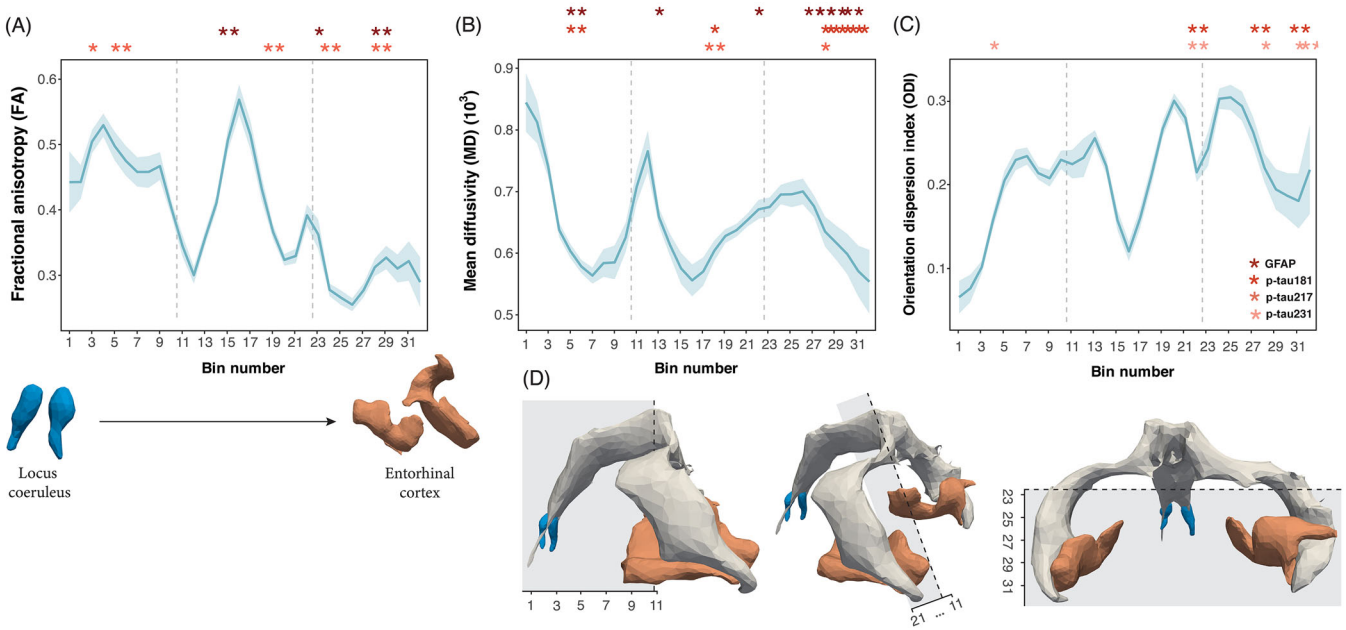

FIGURE 3 (A) FA, (B) MD, and (C) ODI values across LC-EC tract and loci of significance in associations described in main analysis, namely, with GFAP, p-tau181, p-tau217, and p-tau231. The integrity metrics are calculated as mean values across all subjects, with the shaded area representing the 95% confidence interval. Bins result from pooling the slices per three consecutive slices. The vertical dashed lines (A, B, and C) represent the points along the LC-EC tract in which the direction of slicing changed due to a change in the direction of the pathway (D). Statistical significance is indicated as $^{*}p < 0.05$, $^{**}p < 0.01$, $^{***}p < 0.001$. EC, entorhinal cortex; FA, fractional anisotropy; GFAP, glial fibrillary acidic protein; LC, locus coeruleus; MD, mean diffusivity; ODI, orientation dispersion index.

integrity metrics (e.g., axial and radial diffusivity)[7–9] or with higher CSF- or PET-derived measures of tau burden.[10,36] While previous studies examined later disease stages, our results include advanced biophysical diffusion modeling to demonstrate that plasma-derived p-tau pathology is related to early alterations in fiber coherence in asymptomatic individuals. This is compatible with underlying axonal and myelin degeneration processes in vulnerable regions during the preclinical phase and suggests that such pathological processes continue across AD stages. Importantly, the LC-EC tract axons are late and thinly myelinated, which could make them particularly vulnerable to premature axonal injury.[25] Finally, our findings align with a broader range of studies investigating WM integrity in other tracts affected both in preclinical[37] and AD cohorts[7–9,38–42] and demonstrating the role of WM tract health in the deposition or propagation of tau.[43,44] Given the pathway's potential involvement in early tau pathology propagation, our findings suggest the presence of initial WM alterations within a healthy cohort characterized by relatively low levels of amyloid burden.

We identified a positive relationship between ODI and p-tau burden in our cohort. Higher ODI values typically indicate loss of fiber coherence in WM, but recent studies indicated that its interpretation depends on local-, tract-, or population-dependent WM characteristics. Previous work showed higher ODI along with elevated diffusivity and lower anisotropy in MCI patients,[41] whereas another study reported lower WM ODI values in MCI and AD compared to healthy controls, but no differences in FA in the MCI group.[45] This discrepancy may reflect selective sparing or degeneration of crossing fibers, where degradation of secondary fibers within selected voxels would make the primary bundle fibers appear more aligned, thereby increasing axonal coherence and reducing ODI.[46] Our findings in the LC-EC tract indicate that higher ODI is detrimental, as evidenced by the positive relationship between ODI and p-tau burden. Hyperphosphorylation of tau contributes to cytoskeletal destabilization and neurite and axonal disarray.[6] Neuropathological observations show the presence of early hyperphosphorylated tau in LC-related dendrites and long axons,[6] and we speculate that these tau-related morphological changes can be detected as lower microstructural ODI-derived fiber organizational coherence in the LC-EC tract. Of particular interest, the observed positive association between p-tau231 and LC-EC ODI supports the proposition that advanced biophysical diffusion models combined with early biomarkers may capture earlier pathological processes disrupting the structural integrity of the LC-EC tract than standard DTI models.

Second, we observed that lower FA and higher MD in the LC-EC tract corresponded to higher plasma GFAP levels. The LC-NE system is implicated in the modulation of neuroinflammatory processes by downregulating the microglial functions and the transcription of pro-inflammatory genes in astrocytes.[14,47–49] Conversely, destroying LC neurons with the selective noradrenergic neurotoxin N-(2chloroethyl)-N-ethyl-2-bromobenzylamine (DSP-4) led to NE depletion and exacerbated neuroinflammatory responses and astrocyte reactivity in transgenic mice.[50] Reactive astrocytic dysregulation is marked by the overexpression of GFAP, with both animal and human neuropathology studies demonstrating that elevated GFAP levels in aging[51] may contribute to less clearance of Aβ[49] and presence

of both neurofibrillary tangles and Aβ plaques.[52] We now extend these observations by additionally demonstrating that higher GFAP is associated with lower microstructural properties of the LC-EC tract.

In a series of exploratory analyses probing the topographical specificity of the relationships between LC-EC tract integrity and plasma AD-related biomarkers, we found that associations with plasma markers mostly concentrated at the bending points of the tract and toward its terminal portion. Although speculative, the evolution of FA, MD, and ODI values across the LC-EC tract could indicate that local WM integrity disruption reflects local characteristics of sharply bending portions within the bundle, with the parts of the tract exhibiting greater curvature or tissue stiffness being more vulnerable to biomechanical stress.[53] Importantly, these loci display similar robustness in the diffusion measures, as confidence intervals for all metrics are consistent throughout the tract. Besides the expected fanning of fibers as they approach their cortical targets, the observation that WM bundle portions closer to the EC exhibit higher axonal injury compared to the initial, LC-efferent part of the pathway is consistent with the proposed resilience of the LC throughout the development of AD pathology[54] and the neurodegenerative molecular mechanisms determining the selective vulnerability of EC neurons during AD pathogenesis.[55] Furthermore, local differences in the distribution of 4-repeat (4R) and 3-repeat (3R) tau isoforms along the tract might contribute to a higher occurrence of EC-biased associations. The LC harbors pretangle tau inclusions for a prolonged phase during the disease, with pretangle neurons exhibiting 4R-selective immunoreactivity, while the EC might exhibit tau pathology with a higher proportion of 3R isoforms,[56,57] relating differently to neuronal health. The specificity of our results is further corroborated by the control tract analysis, showing no significant associations between microstructural integrity metrics and tau pathology or astrogliosis. In contrast, WM degeneration in these (pre-)frontal regions was associated only with plasma amyloid burden, consistent with the topography of Aβ.[58,59]

Our study has several strengths. First, previous studies focusing on the structural integrity of the LC-EC pathway in patients along the AD continuum[7–9] used a normative atlas of the tract, and they either examined a clinical cohort[7,8] or considered previously diagnosed preclinical stages, with no explicit information on the range in underlying pathological burden.[9] Our study combined recently developed plasma AD markers and dedicated ultra-high-field LC imaging, allowing us to identify the LC and track the LC-EC pathway at the individual level with an improved resolution, and the incorporation of advanced NODDI modeling alongside traditional DTI modeling to facilitate the interpretation of[13] different neurobiological processes.[21] However, our study also has limitations. First, our biomarker quantification method lacks spatial specificity when compared to similar assessments using PET, preventing us from drawing conclusions about the tau topography in the cortex. However, plasma markers are likely more sensitive in earlier stages as they also capture soluble forms, which is particularly important when investigating the earliest tau-related changes to the LC. Second, despite the uniqueness of the ultra-high-field MRI data and dedicated LC sequences, our dataset was relatively small, resulting in several marginally significant results after the FDR correction. Therefore, these results need to be interpreted with caution and require replication in future studies using a larger sample size. Finally, our cross-sectional approach limits causal interpretation, and our research question would benefit from a longitudinal framework to better elucidate the temporal ordering of the events at play.

5 | CONCLUSION

In conclusion, we provide in vivo evidence that elevated tau burden and astrocyte reactivity are associated with lower structural integrity within the LC-EC tract, marked by axonal degeneration and fiber disorganization. To our knowledge, this study is among the first investigating the LC-EC tract integrity in a healthy cohort with availability of both ultra-high-field imaging data and multiple plasma AD-related biomarkers. Our results show that microstructural alterations of the LC-EC tract reveal insights into the earliest AD-related pathophysiological processes, which may hold promise in identifying individuals at risk of progressing along the AD trajectory.

ACKNOWLEDGMENTS

Yuliya Patsyuk (Conceptualization, Methodology, Formal analysis, Visualization, Writing – original draft, Writing – review and editing), Maxime Van Egroo (Conceptualization, Methodology, Supervision, Writing – original draft, Writing – review and editing), Elise Beckers (Methodology, Writing – review and editing), Elouise A. Koops (Methodology, Writing – review and editing), Nicholas J. Ashton (Methodology, Writing – review and editing), Shorena Janelidze (Methodology, Writing – review and editing), Kaj Blennow (Methodology, Writing – review and editing), Oskar Hansson (Methodology, Writing – review and editing), Henrik Zetterberg (Methodology, Writing – review and editing), Benedikt A. Poser (Writing – review and editing), and Heidi I. L. Jacobs (Conceptualization, Funding acquisition, Project administration, Supervision, Writing – original draft, Writing – review and editing). This work was supported by Alzheimer Nederland (WE.03-2019-02, Heidi I. L. Jacobs), Alzheimer's Association (AARG-22-920434, Heidi I. L. Jacobs) and the BrightFocus Foundation (A20211016F, Maxime Van Egroo). Maxime Van Egroo is supported by European Union's Marie Skłodowska-Curie Actions (101109451-ADEEPSLEEP). Kaj Blennow is supported by the Swedish Research Council (2017–00915), the Alzheimer Drug Discovery Foundation (ADDF), USA (RDAPB-201809-2016615), the Swedish Alzheimer Foundation (AF-930351, AF-939721, and AF-968270), Hjärnfonden, Sweden (FO2017-0243 and ALZ2022-0006), the Swedish state under the agreement between the Swedish government and the County Councils, the ALF-agreement (ALFGBG-715986 and ALFGBG-965240), the European Union Joint Program for Neurodegenerative Disorders (JPND2019-466-236), the National Institute of Health (NIH), USA, (grant 1R01AG068398-01), and the Alzheimer's Association 2021 Zenith Award (ZEN-21-848495). Oskar Hansson is supported by the Swedish Research Council (2016–00906), the Knut and Alice Wallenberg foundation (2017–0383), the Marianne and Marcus Wallenberg Foundation (2015.0125), the Strategic

Research Area MultiPark (Multidisciplinary Research in Parkinson's disease) at Lund University, the Swedish Alzheimer Foundation (AF-939932), the Swedish Brain Foundation (FO2021–0293), Parkinson Foundation of Sweden (1280/20), the Cure Alzheimer's Fund, the Konung Gustaf V:s och Drottning Victorias Frimurarestiftelse, the Skåne University Hospital Foundation (2020-O000028), Regionalt Forskningsstöd (2020–0314), and the Swedish federal government under an ALF agreement (2018-Projekt0279). Henrik Zetterberg is a Wallenberg Scholar and a Distinguished Professor at the Swedish Research Council supported by grants from the Swedish Research Council (2023–00356; 2022–01018, and 2019–02397), the European Union's Horizon Europe Research and Innovation Programme under grant agreement no. 101053962, Swedish State Support for Clinical Research (ALFGBG-71320), the Alzheimer Drug Discovery Foundation (ADDF), USA (201809–2016862), the AD Strategic Fund and the Alzheimer's Association (ADSF-21-831376-C, ADSF-21-831381-C, ADSF-21-831377-C, and ADSF-24-1284328-C), the Bluefield Project, Cure Alzheimer's Fund, the Olav Thon Foundation, the Erling-Persson Family Foundation, Stiftelsen för Gamla Tjänarinnor, Hjärnfonden, Sweden (FO2022-0270), the European Union's Horizon 2020 Research and Innovation Programme under the Marie Skłodowska-Curie grant agreement no. 860197 (MIRIADE), the European Union Joint Programme—Neurodegenerative Disease Research (JPND2021-00694), the National Institute for Health and Care Research University College London Hospitals Biomedical Research Centre, and the UK Dementia Research Institute at UCL (UKDRI-1003). Elouise A. Koops is supported by an Alzheimer's Association Research Fellowship (23AARF-1026796). Benedikt A. Poser is supported by H2020 FET-Open AROMA grant agreement no. 88587. Heidi I. L. Jacobs is supported by NIH grants R01AG062559, R01AG06806, R01AG082006, and R21AG074220.

CONFLICT OF INTEREST STATEMENT

Elouise A. Koops is the program chair of the Neuromodulatory Subcortical Systems Professional Interest Area of ISTAART. Nicholas J. Ashton has given lectures in symposia sponsored by Eli Lilly and is an associate editor at Alzheimer's Research & Therapy. Kaj Blennow has served as a consultant, on advisory boards, or on data monitoring committees for Abcam, Axon, BioArctic, Biogen, JOMDD/Shimadzu, Julius Clinical, Lilly, MagQu, Novartis, Ono Pharma, Pharmatrophix, Prothena, Roche Diagnostics, and Siemens Healthineers, is a co-founder of Brain Biomarker Solutions in Gothenburg AB (BBS), which is a part of the GU Ventures Incubator Program (outside submitted work), and is a member of the editorial board at *Alzheimer's Research & Therapy*. Oskar Hansson is an employee of Lund University and Eli Lilly. Henrik Zetterberg has served on scientific advisory boards and/or as a consultant for AbbVie, Acumen, Alector, Alzinova, ALZpath, Amylyx, Annexon, Apellis, Artery Therapeutics, AZTherapies, Cognito Therapeutics, CogRx, Denali, Eisai, Enigma, LabCorp, Merck Sharp & Dohme, Merry Life, Nervgen, Novo Nordisk, Optoceutics, Passage Bio, Pinteon Therapeutics, Prothena, Quanterix, Red Abbey Labs, reMYND, Roche, Samumed, ScandiBio Therapeutics AB, Siemens Healthineers, Triplet Therapeutics, and Wave, has given lectures sponsored by Alzecure, BioArctic, Biogen, Cellectricon, Fujirebio, LabCorp, Lilly, Novo Nordisk, Oy Medix Biochemica AB, Roche, and WebMD, is a co-founder of Brain Biomarker Solutions in Gothenburg AB (BBS), which is a part of the GU Ventures Incubator Program, and is a shareholder of MicThera (outside submitted work). Heidi I. L. Jacobs is immediate past chair of the Neuromodulatory Subcortical Systems Professional Interest Area of ISTAART and served as advisory board member of ISTAART. These relationships are not related to the content of the manuscript. All other authors report no relevant conflicts. Author disclosures are available in the Supporting Information.

CONSENT STATEMENT

The study was conducted in accordance with the Declaration of Helsinki, and the experimental protocol was approved by the local Medical Ethics Committee of the Maastricht University Medical Center. Written informed consent was obtained from all the participants prior to inclusion.

REFERENCES

1. Sara SJ. The locus coeruleus and noradrenergic modulation of cognition. *Nat Rev Neurosci*. 2009;10(3):211–223. doi:10.1038/nrn2573
2. Braak H, Thal DR, Ghebremedhin E, Del Tredici K. Stages of the pathologic process in Alzheimer disease: age categories from 1 to 100 years. *J Neuropathol Exp Neurol*. 2011;70(11):960–969. doi:10.1097/NEN.0b013e318232a379
3. Hary AT, Chadha S, Mercaldo N, et al. Locus coeruleus tau validates and informs high-resolution MRI in aging and at earliest Alzheimer's pathology stages. *Acta Neuropathol Commun*. 2025;13(1):44. doi:10.1186/s40478-025-01957-6
4. Stratmann K, Heinsen H, Korf HW, et al. Precortical phase of Alzheimer's disease (AD)-related tau cytoskeletal pathology. *Brain Pathol*. 2016;26(3):371–386. doi:10.1111/bpa.12289
5. Braak H, Del Tredici K. Alzheimer's pathogenesis: is there neuron-to-neuron propagation? *Acta Neuropathol*. 2011;121(5):589–595. doi:10.1007/s00401-011-0825-z
6. Gilvesy A, Husen E, Magloczky Z, et al. Spatiotemporal characterization of cellular tau pathology in the human locus coeruleus–pericoerulear complex by three-dimensional imaging. *Acta Neuropathol*. 2022;144(4):651–676. doi:10.1007/s00401-022-02477-6
7. Chu WT, Wang W-E, Zaborszky L, et al. Association of cognitive impairment with free water in the nucleus basalis of meynert and locus coeruleus to transentorhinal cortex tract. *Neurology*. 2022;98(7):e700–e710. doi:10.1212/WNL.0000000000013206
8. Quattrini G, Pini L, Boscolo Galazzo I, et al. Microstructural alterations in the locus coeruleus-entorhinal cortex pathway in Alzheimer's disease and frontotemporal dementia. *Alzheimers Dement (Amst)*. 2024;16(1):e12513. doi:10.1002/dad2.12513
9. Sun W, Tang Y, Qiao Y, et al. A probabilistic atlas of locus coeruleus pathways to transentorhinal cortex for connectome imaging in Alzheimer's disease. *NeuroImage*. 2020;223:117301. doi:10.1016/j.neuroimage.2020.117301
10. Aiello M, Marizzoni M, Borrelli P, et al. Microstructural assessment of the locus coeruleus–entorhinal cortex pathway and association with ATN markers in cognitive impairment. *Alzheimers Dement*. 2025;21(4):e70126. doi:10.1002/alz.70126
11. Engels-Domínguez N, Koops EA, Prokopiou PC, et al. State-of-the-art imaging of neuromodulatory subcortical systems in aging and Alzheimer's disease: challenges and opportunities. *Neurosci Biobehav Rev*. 2023;144:104998. doi:10.1016/j.neubiorev.2022.104998

12. Priovoulos N, Jacobs HIL, Ivanov D, Uludağ K, Verhey FRJ, Poser BA. High-resolution in vivo imaging of human locus coeruleus by magnetization transfer MRI at 3T and 7T. *NeuroImage*. 2018;168:427–436. doi:10.1016/j.neuroimage.2017.07.045
13. Zhang H, Schneider T, Wheeler-Kingshott CA, Alexander DC. NODDI: practical in vivo neurite orientation dispersion and density imaging of the human brain. *NeuroImage*. 2012;61(4):1000–1016. doi:10.1016/j.neuroimage.2012.03.072
14. Beckers E, Egroo MV, Ashton NJ, et al. Microstructural associations between locus coeruleus, cortical, and subcortical regions are modulated by astrocyte reactivity: a 7T MRI adult lifespan study. *Cereb Cortex*. 2024;34(6):bhae261. doi:10.1093/cercor/bhae261
15. Van Egroo M, van Hooren RWE, Jacobs HIL. Associations between locus coeruleus integrity and nocturnal awakenings in the context of Alzheimer's disease plasma biomarkers: a 7T MRI study. *Alzheimers Res Ther*. 2021;13(1):159. doi:10.1186/s13195-021-00902-8
16. Van Egroo M, Riphagen JM, Ashton NJ, et al. Ultra-high field imaging, plasma markers and autopsy data uncover a specific rostral locus coeruleus vulnerability to hyperphosphorylated tau. *Mol Psychiatry*. 2023;2023:1–11. doi:10.1038/s41380-023-02041-y. Published online April 5.
17. Marques JP, Kober T, Krueger G, van der Zwaag W, Van de Moortele PF, Gruetter R. MP2RAGE, a self-bias-field corrected sequence for improved segmentation and T1-mapping at high field. *NeuroImage*. 2010;49(2):1271–1281. doi:10.1016/j.neuroimage.2009.10.002
18. Fischl B. FreeSurfer. *NeuroImage*. 2012;62(2):774–781. doi:10.1016/j.neuroimage.2012.01.021
19. Dale AM, Fischl B, Sereno MI. Cortical surface-based analysis: I. Segmentation and surface reconstruction. *NeuroImage*. 1999;9(2):179-194. doi:10.1006/nimg.1998.0395
20. Jenkinson M, Beckmann CF, Behrens TEJ, Woolrich MW, Smith SM. FSL. *NeuroImage*. 2012;62(2):782–790. doi:10.1016/j.neuroimage.2011.09.015
21. Beaulieu C. CHAPTER 6-the biological basis of diffusion anisotropy. In: Johansen-Berg H, Behrens TEJ, eds. *Diffusion MRI*. Academic Press; 2009:105–126. doi:10.1016/B978-0-12-374709-9.00006-7
22. Desikan RS, Ségonne F, Fischl B, et al. An automated labeling system for subdividing the human cerebral cortex on MRI scans into gyral based regions of interest. *NeuroImage*. 2006;31(3):968–980. doi:10.1016/j.neuroimage.2006.01.021
23. Ashton NJ, Pascoal TA, Karikari TK, et al. Plasma p-tau231: a new biomarker for incipient Alzheimer's disease pathology. *Acta Neuropathol*. 2021;141(5):709–724. doi:10.1007/s00401-021-02275-6
24. Janelidze S, Berron D, Smith R, et al. Associations of plasma phospho-tau217 levels with tau positron emission tomography in early Alzheimer disease. *JAMA Neurol*. 2021;78(2):149–156. doi:10.1001/jamaneurol.2020.4201
25. Braak H, Del Tredici K. The preclinical phase of the pathological process underlying sporadic Alzheimer's disease. *Brain*. 2015;138(10):2814–2833. doi:10.1093/brain/awv236
26. Bueichekú E, Diez I, Kim CM, et al. Spatiotemporal patterns of locus coeruleus integrity predict cortical tau and cognition. *Nat Aging*. 2024;4(5):625–637. doi:10.1038/s43587-024-00626-y
27. Ehrenberg AJ, Nguy AK, Theofilas P, et al. Quantifying the accretion of hyperphosphorylated tau in the locus coeruleus and dorsal raphe nucleus: the pathological building blocks of early Alzheimer's disease. *Neuropathol Appl Neurobiol*. 2017;43(5):393–408. doi:10.1111/nan.12387
28. Iba M, McBride JD, Guo JL, Zhang B, Trojanowski JQ, Lee VMY. Tau pathology spread in PS19 tau transgenic mice following locus coeruleus (LC) injections of synthetic tau fibrils is determined by the LC's afferent and efferent connections. *Acta Neuropathol*. 2015;130(3):349–362. doi:10.1007/s00401-015-1458-4
29. Ghosh A, Torraville SE, Mukherjee B, et al. An experimental model of Braak's pretangle proposal for the origin of Alzheimer's disease: the role of locus coeruleus in early symptom development. *Alzheimers Res Ther*. 2019;11(1):59. doi:10.1186/s13195-019-0511-2
30. Lantero Rodriguez J, Karikari TK, Suárez-Calvet M, et al. Plasma p-tau181 accurately predicts Alzheimer's disease pathology at least 8 years prior to postmortem and improves the clinical characterization of cognitive decline. *Acta Neuropathol*. 2020;140(3):267–278. doi:10.1007/s00401-020-02195-x
31. Lehmann S, Schraen-Maschke S, Vidal JS, et al. Plasma phosphorylated-tau181 predicts amyloid status and conversion to dementia stage dependent on renal function. *J Neurol Neurosurg Psychiatry*. 2023;94(6):411–419. doi:10.1136/jnnp-2022-330540
32. Milà-Alomà M, Ashton NJ, Shekari M, et al. Publisher Correction: plasma p-tau231 and p-tau217 as state markers of amyloid-β pathology in preclinical Alzheimer's disease. *Nat Med*. 2022;28(9):1965–1965. doi:10.1038/s41591-022-02037-1
33. Bayoumy S, Verberk IMW, den Dulk B, et al. Clinical and analytical comparison of six Simoa assays for plasma p-tau isoforms p-tau181, p-tau217, and p-tau231. *Alzheimers Res Ther*. 2021;13(1):198. doi:10.1186/s13195-021-00939-9
34. Mattsson-Carlgren N, Janelidze S, Palmqvist S, et al. Longitudinal plasma p-tau217 is increased in early stages of Alzheimer's disease. *Brain*. 2020;143(11):3234–3241. doi:10.1093/brain/awaa286
35. Ercan-Herbst E, Ehrig J, Schöndorf DC, et al. A post-translational modification signature defines changes in soluble tau correlating with oligomerization in early-stage Alzheimer's disease brain. *Acta Neuropathol Commun*. 2019;7:192. doi:10.1186/s40478-019-0823-2
36. Solders SK, Galinsky VL, Clark AL, et al. Diffusion MRI tractography of the locus coeruleus-transentorhinal cortex connections using GO-ESP. *Magn Reson Med*. 2022;87(4):1816–1831. doi:10.1002/mrm.29088
37. Jacobs HIL, Hedden T, Schultz AP, et al. Structural tract alterations predict downstream tau accumulation in amyloid-positive older individuals. *Nat Neurosci*. 2018;21(3):424–431. doi:10.1038/s41593-018-0070-z
38. Bozzali M, Falini A, Franceschi M, et al. White matter damage in Alzheimer's disease assessed in vivo using diffusion tensor magnetic resonance imaging. *J Neurol Neurosurg Psychiatry*. 2002;72(6):742–746. doi:10.1136/jnnp.72.6.742
39. Kantarci K, Murray ME, Schwarz CG, et al. White-matter integrity on DTI and the pathologic staging of Alzheimer's disease. *Neurobiol Aging*. 2017;56:172–179. doi:10.1016/j.neurobiolaging.2017.04.024
40. Medina D, DeToledo-Morrell L, Urresta F, et al. White matter changes in mild cognitive impairment and AD: a diffusion tensor imaging study. *Neurobiol Aging*. 2006;27(5):663–672. doi:10.1016/j.neurobiolaging.2005.03.026
41. Wen Q, Mustafi SM, Li J, et al. White matter alterations in early-stage Alzheimer's disease: a tract-specific study. *Alzheimers Dement (Amst)*. 2019;11:576–587. doi:10.1016/j.dadm.2019.06.003
42. Zhang Y, Schuff N, Jahng GH, et al. Diffusion tensor imaging of cingulum fibers in mild cognitive impairment and Alzheimer disease. *Neurology*. 2007;68(1):13–19. doi:10.1212/01.wnl.0000250326.77323.01
43. Araque Caballero MÁ, Suárez-Calvet M, Duering M, et al. White matter diffusion alterations precede symptom onset in autosomal dominant Alzheimer's disease. *Brain J Neurol*. 2018;141(10):3065–3080. doi:10.1093/brain/awy229
44. Nabizadeh F, Pourhamzeh M, Khani S, et al. Plasma phosphorylated-tau181 levels reflect white matter microstructural changes across Alzheimer's disease progression. *Metab Brain Dis*. 2022;37(3):761–771. doi:10.1007/s11011-022-00908-7
45. Fu X, Shrestha S, Sun M, et al. Microstructural white matter alterations in mild cognitive impairment and Alzheimer's disease. *Clin Neuroradiol*. 2020;30(3):569–579. doi:10.1007/s00062-019-00805-0
46. Wearn A, Tremblay SA, Tardif CL, et al. Neuromodulatory subcortical nucleus integrity is associated with white matter microstructure,

tauopathy and APOE status. *Nat Commun*. 2024;15(1):4706. doi:10.1038/s41467-024-48490-z
47. Braun D, Madrigal JLM, Feinstein DL. Noradrenergic regulation of glial activation: molecular mechanisms and therapeutic implications. *Curr Neuropharmacol*. 2014;12(4):342–352. doi:10.2174/1570159X12666140828220938
48. Finnell JE, Moffitt CM, Hesser LA, et al. The contribution of the locus coeruleus-norepinephrine system in the emergence of defeat-induced inflammatory priming. *Brain Behav Immun*. 2019;79:102–113. doi:10.1016/j.bbi.2019.01.021
49. Heneka MT, Nadrigny F, Regen T, et al. Locus coeruleus controls Alzheimer's disease pathology by modulating microglial functions through norepinephrine. *Proc Natl Acad Sci U S A*. 2010;107(13):6058–6063. doi:10.1073/pnas.0909586107
50. Heneka MT, Ramanathan M, Jacobs AH, et al. Locus coeruleus degeneration promotes Alzheimer pathogenesis in amyloid precursor protein 23 transgenic mice. *J Neurosci Off J Soc Neurosci*. 2006;26(5):1343–1354. doi:10.1523/JNEUROSCI.4236-05.2006
51. Nichols NR, Day JR, Laping NJ, Johnson SA, Finch CE. GFAP mRNA increases with age in rat and human brain. *Neurobiol Aging*. 1993;14(5):421–429. doi:10.1016/0197-4580(93)90100-p
52. Porchet R, Probst A, Bouras C, Dráberová E, Dráber P, Riederer BM. Analysis of glial acidic fibrillary protein in the human entorhinal cortex during aging and in Alzheimer's disease. *Proteomics*. 2003;3(8):1476–1485. doi:10.1002/pmic.200300456
53. Pillai EK, Franze K. Mechanics in the nervous system: from development to disease. *Neuron*. 2024;112(3):342–361. doi:10.1016/j.neuron.2023.10.005
54. Theofilas P, Ehrenberg AJ, Dunlop S, et al. Locus coeruleus volume and cell population changes during Alzheimer's disease progression: a stereological study in human postmortem brains with potential implication for early-stage biomarker discovery. *Alzheimers Dement*. 2017;13(3):236–246. doi:10.1016/j.jalz.2016.06.2362
55. Olajide OJ, Suvanto ME, Chapman CA. Molecular mechanisms of neurodegeneration in the entorhinal cortex that underlie its selective vulnerability during the pathogenesis of Alzheimer's disease. *Biol Open*. 2021;10(1):bio056796. doi:10.1242/bio.056796
56. Hara M, Hirokawa K, Kamei S, Uchihara T. Isoform transition from four-repeat to three-repeat tau underlies dendrosomatic and regional progression of neurofibrillary pathology. *Acta Neuropathol*. 2013;125(4):565–579. doi:10.1007/s00401-013-1097-6
57. Uematsu M, Nakamura A, Ebashi M, Hirokawa K, Takahashi R, Uchihara T. Brainstem tau pathology in Alzheimer's disease is characterized by increase of three repeat tau and independent of amyloid *β*. *Acta Neuropathol Commun*. 2018;6(1):1. doi:10.1186/s40478-017-0501-1
58. Braak H, Braak E. Neuropathological stageing of Alzheimer-related changes. *Acta Neuropathol*. 1991;82(4):239–259. doi:10.1007/BF00308809
59. Thal DR, Rüb U, Orantes M, Braak H. Phases of A*β*-deposition in the human brain and its relevance for the development of AD. *Neurology*. 2002;58(12):1791–1800. doi:10.1212/wnl.58.12.1791

SUPPORTING INFORMATION

Additional supporting information can be found online in the Supporting Information section at the end of this article.

How to cite this article: Patsyuk Y, Van Egroo M, Beckers E, et al. Locus coeruleus-entorhinal cortex tract integrity is linked to plasma tau and glial fibrillary acidic protein. *Alzheimer's Dement*. 2025;21:e70915. https://doi.org/10.1002/alz.70915